RSC Advances

ROYAL SOCIETY OF CHEMISTRY

www.rsc.org/advances

Journal Name

ARTICLE

In Situ Template-Free Synthesis of a Novel 3D p-n Heteroarchitecture Ag_3PO_4/Ta_3N_5 Photocatalyst with High Activity and Stability under Visible Radiation

Received 00th January 20xx,
Accepted 00th January 20xx

DOI: 10.1039/x0xx00000x

www.rsc.org/

Wen Wang,[a] Hua-Bin Fang,[a] Yan-Zhen Zheng,*[a,b] Yanke Che, Xia Tao,*[a] and Jian-Feng Chen[b]

A novel 3D p–n heteroarchitecture Ag_3PO_4/Ta_3N_5 composite photocatalyst with double visible-light-response characteristics has been prepared using an in-situ template-free precipitation method. It is found that the fascinating Ag_3PO_4/Ta_3N_5 exhibited high superior photoactivity and photostability compared to bare Ag_3PO_4 and Ta_3N_5 for the degradation of RhB under visible light irradiation. The improved performance of the composite is primarily attributable to sufficient visible-light harvesting, efficient charge separation and transfer of photogenerated electrons and holes resulting from matched energy bandgaps and sufficient p-n hetero-interfaces between Ag_3PO_4 and Ta_3N_5. The quenching effects of different scavengers demonstrate that the reactive h^+ and $O_2^{-\bullet}$ species played a major role in the photodegradation process. It is expected that the 3D p–n heterostructure composite fabricating via a facile precipitation method, may be a promising candidate for organic pollutant degradation.

Introduction

Visible-light photocatalysis, which can directly harvest energy from incoming solar energy offers a desirable method for solving the issues of energy shortage and environmental remediation.[1,2] Currently, numerous visible-light-driven photocatalysts, such as doped semiconductors, as well as multiple-metal oxides including Ag,[3-5] Bi,[6-8] and In-based[9,10] semiconductors, have been developed for photocatalytic water-splitting and photocatalytic degradation of organics in the air and wastewater. Among these photocatalysts, silver orthophosphate (Ag_3PO_4; Eg = 2.45 eV), which was reported by Ye and coworkers,[11,12] exhibited extremely high photooxidative capabilities for O_2 evolution from water as well as organic dye decomposition under visible light irradiation. However, Ag_3PO_4 suffers from poor photostability in practical applications because it readily decomposes photochemically when no sacrificial reagent is involved.[13] The development of photocatalysts with sufficient charge separation capability and high photocatalytic stability in the visible region is still the most challenging task in Ag_3PO_4 based photocatalysis research. The formation of a heterojunction between two semiconductors is an effective strategy for enhancing the separation of photogenerated electron-hole pairs.[14] Recently, some composite photocatalysts based on Ag_3PO_4, such as AgX/Ag_3PO_4 (X = Cl, Br, I), Ag_3PO_4/TiO_2, Ag_3PO_4/Fe_3O_4, Ag_3PO_4/SnO_2 and graphene oxide/Ag_3PO_4 have been fabricated and exhibited enhanced photocatalytic activity and stability compared to the pure Ag_3PO_4 catalyst.[11,15-18] These results indicate that tailoring and fabricating the phase interface/junctions between the light harvesting semiconductors can effectively improve the stability and reduce the photocorrosion of Ag_3PO_4 photocatalysts.

(Oxy)nitride materials with a narrow band gap and a more negative potential for the nitrogen 2p orbital (i.e., $TiO_{2-x}N_x$, Ta_3N_5, TaON, $LaTiO_2N$, and GaN:ZnO) have been extensively developed to induce the photocatalytic reaction under visible light irradiation.[19-24] Tantalum nitride (Ta_3N_5) is one of the most promising photocatalysts for solar energy conversion via water splitting because it has a suitable band gap of 2.1 eV and appropriate band edge positions. The maximum solar-to-hydrogen efficiency of the Ta_3N_5 photoelectrode is as high as 15.9% under AM 1.5 G radiation.[25] However, due to the self-oxidative decomposition of Ta_3N_5 in which nitrogen anions are oxidized to N_2 by photogenerated holes, the photocatalytic activity of bare Ta_3N_5 is on the decreases during photocatalytic water splitting.[25] For example, the reported half-value period of the photocurrent for IrO_2-loaded Ta_3N_5 was estimated to be less than 10 minutes, indicating that the stability remains very poor for photocatalytic water splitting.[26] Therefore, prompt separation of the photogenerated electrons and holes is crucial for enhancing the activity and stability of the Ta_3N_5 catalyst. The p-n junction is one design concept for separating the electrons and holes using internal build-in fields induced by band bending.[14] The concept, which originated from the design of high-performance solar cells, has been successfully adopted for fabrication of semiconductor

[a] State Key Laboratory of Organic-Inorganic Composites, Beijing University of Chemical Technology, Beijing 100029 , P. R. China. E-mail: taoxia@yahoo.com
[b] Research Center of the Ministry of Education for High Gravity Engineering & Technology, Beijing University of Chemical Technology, Beijing 100029 , P. R. China
[c] Beijing National Laboratory for Molecular Sciences, Key Laboratory of Photochemistry, Institute of Chemistry, Chinese Academy of Sciences, Beijing 100190, P. R. China

† Electronic Supplementary Information (ESI) available: EDS mapping images of the Ag3PO4/Ta3N5 photocatalyst, Plot of $(Ahv)^2$ versus Eg, UV-Vis spectra changes in the degradation of RhB with Ag_3PO_4/Ta_3N_5. See DOI: 10.1039/x0xx00000x

photocatalysts.[27] However, because p-type semiconductor oxides are rather rare, only a few p–n heterojunction photocatalysts have been selectively studied so far, such as Co_3O_4/Ta_3N_5 and ZrO_2/Ta_3N_5.[28,29]

Judging from their respective nature and photocatalytic activity of two visible-light-driven photocatalysts as mentioned above i.e. p-type Ag_3PO_4 and n-type Ta_3N_5 as well as the possibility of forming p-n heterojunction in the interface of the two species, the combination of Ag_3PO_4 and n-type Ta_3N_5 seems to be ideal for the effective separation and transfer of electrons and holes, and consequently improving the photocatalytic efficiency and photostability of the composite photocatalyst. In this paper, we report for the first time the synthesis of 3D heteroarchitectured visible-light-driven p–n heterojunction Ag_3PO_4/Ta_3N_5 photocatalyst by a facile in-situ template-free precipitation method. As anticipated, the as-obtained 3D heteroarchitectured composite photocatalyst exhibited extremely high photocatalytic performance and photostability that is superior to bare Ag_3PO_4 and Ta_3N_5 toward degradation of rhodamine B (RhB) under visible-light irradiation (≥420 nm). The enhanced performance is discussed in detail based on the inherent nature of heteroarchitecture Ag_3PO_4/Ta_3N_5 as well as its spectral characterizations and photoelectrochemical measurements. A possible photodegradation mechanism is also proposed.

Results and discussion

In situ growth of Ag_3PO_4/Ta_3N_5 composite

Direct precipitation growth is commonly used to fabricate different kinds of composite. In the present work, an in situ precipitation method is adopted for the synthesis of the Ag_3PO_4/Ta_3N_5 composite and the synthesis procedure is schematically shown in Fig. 1. Specifically, Ta_3N_5 nanorod aggregates first obtained via a hydrothermal process was mixed with the precursor for Ag_3PO_4, silver nitrate. As such, the Ag^+ ions could be readily absorbed on the surface of negatively-charged Ta_3N_5 nanorod aggregates by the electrostatic adsorption to form a compact hetero-interface between the two species. Then, the adsorbed Ag^+ reacted with PO_4^{3-} slowly released from bulk HPO_4^{2-} solution to convert into Ag_3PO_4 particles on the surface of Ta_3N_5 nanorod aggregates under constant stirring at room temperature. In the process of subsequent reaction Ag_3PO_4 particles deposited on the surface of the Ta_3N_5 nanorod aggregates grew up gradually, with size enlarging from nanometer-scale to submicron-sized hierarchical scale. This in situ precipitation method for the synthesis of an Ag_3PO_4/Ta_3N_5 hybrid composite photocatalyst can also be summarized as follows:

$$Ag^+(aq) + Ta_3N_5 \rightarrow Ag^+/Ta_3N_5 \quad (1)$$

$$Ag^+/Ta_3N_5 + PO_4^{3-}(aq) \rightarrow Ag_3PO_4/Ta_3N_5 \quad (2)$$

Characterization of Ag_3PO_4/Ta_3N_5 photocatalyst

The phase purity and crystal structure of the as-synthesized Ag_3PO_4, Ta_3N_5, and Ag_3PO_4/Ta_3N_5 composites were confirmed by XRD characterization. As shown in Fig. 2, all of the diffraction peaks for Ag_3PO_4 and Ta_3N_5 can be readily indexed to body-centered cubic Ag_3PO_4 (JCPDS No.06-0505) and orthorhombic Ta_3N_5 (JCPDS No.79-1533). The results for the Ag_3PO_4/Ta_3N_5 composites indicated the coexistence of both the Ag_3PO_4 and Ta_3N_5 phases, and no other crystal phases were observed in the XRD patterns, suggesting the high purity of the Ag_3PO_4/Ta_3N_5 composite.

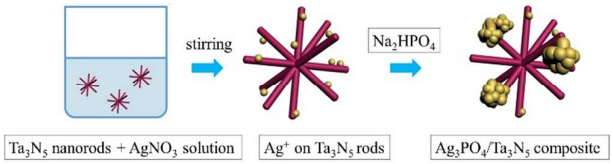

Fig. 1 Schematic diagram of the growth process of Ag_3PO_4/Ta_3N_5.

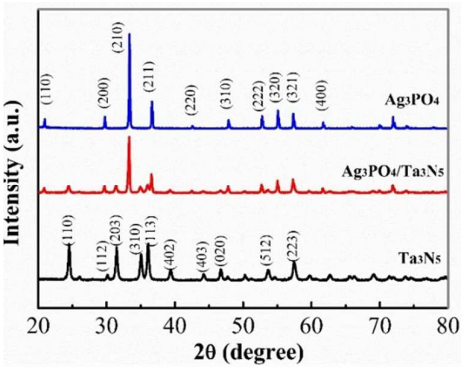

Fig. 2 XRD patterns of the Ag_3PO_4, Ta_3N_5, and Ag_3PO_4/Ta_3N_5 photocatalysts.

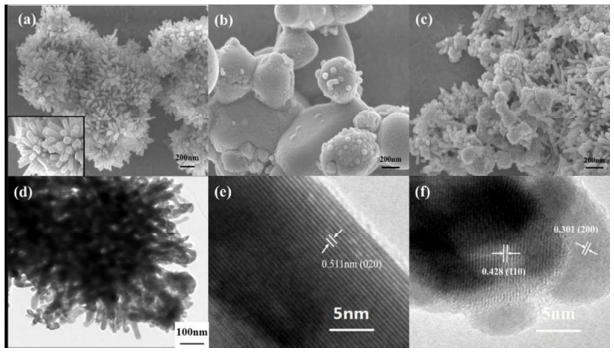

Fig. 3 SEM images of the a) Ta_3N_5, b) Ag_3PO_4 and c) Ag_3PO_4/Ta_3N_5 photocatalysts, TEM image of d) Ag_3PO_4/Ta_3N_5 and HRTEM images of e) Ta_3N_5 and f) Ag_3PO_4 in the Ag_3PO_4/Ta_3N_5 photocatalysts.

The morphology and microstructure of Ag_3PO_4/Ta_3N_5 were characterized by SEM and TEM. As shown in Figure 3a-c, the micro-sized secondary Ta_3N_5 aggregates are composed of numerous primary nanorods with diameters of 40–60 nm and lengths of 200–300 nm (Fig. 3a). The Ag_3PO_4 particles exhibit an irregular spherical-like structure with an integral size ranging from 300 nm to

1.0 μm, and some of the granules adhered to the surface of submicron–sized Ag_3PO_4 (Fig. 3b). Indeed, a number of large-sized Ag_3PO_4 with several to tens of nanometers have also been observed in other reported Ag_3PO_4 based composite photocatalysts.[30] After Ag_3PO_4 particles grown on the surface of the Ta_3N_5 nanorods, one can observe that the size of Ag_3PO_4 decreases remarkably in the hybrid Ag_3PO_4/Ta_3N_5 composite (Fig. 3c). The average size of Ag_3PO_4 particles is in the range of 70–300 nm, which is much smaller than that of the pure Ag_3PO_4 sample. The reason is that the primary Ta_3N_5 nanorods carry negative charge (zeta potential = –39.8 mV, aqueous media) that allows offering sufficient nucleate sites for Ag_3PO_4 precipitation, and thus effectively prevent the formation of micron-sized Ag_3PO_4 bulks. Furthermore, it is worth noting that the 70–300 nm-sized secondary Ag_3PO_4 particle is spherical in shape and made of packed nanocrystallites with 10–20 nm in diameter, as shown in SEM image of Ag_3PO_4/Ta_3N_5 hybrid composite (Fig. 3c). Such 3D hierarchical structures of the composite facilitates forming a rough surface and thus provide sufficient hetero-interfaces for photocatalytic reaction. The magnified image shown in Figure 3d shows the Ta_3N_5 nanorod aggregates to point outward coupling with the dispersed Ag_3PO_4 nanocrystals. The corresponding HRTEM images of the Ag_3PO_4/Ta_3N_5 composites show the distinct crystallographic planes of Ag_3PO_4 (Fig. 3e) and Ta_3N_5 (Fig. 3f), in which a lattice spacing of 0.511 nm corresponds to the (020) plane of the orthorhombic Ta_3N_5 phase and the lattice spacings of 0.428 and 0.301 nm correspond to the (110) and (200) planes of the cubic Ag_3PO_4 phase. EDS mapping images further confirmed the successful preparation of the Ag_3PO_4/Ta_3N_5 composite (Fig. S1).

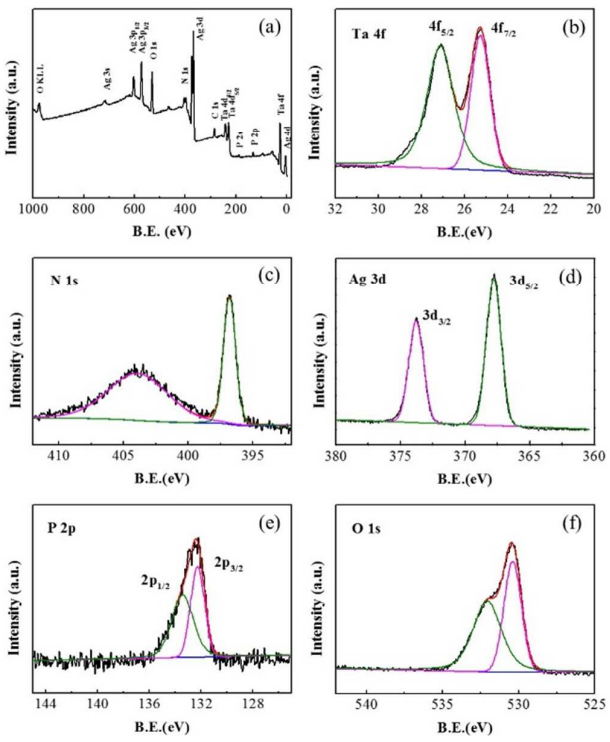

Fig. 4 XPS spectra of Ag_3PO_4/Ta_3N_5 photocatalysts.

X-ray photoelectron spectroscopy (XPS) was also carried out to further investigate the composition and chemical status of the Ag_3PO_4/Ta_3N_5 heterostructure photocatalyst, and the results are shown in the Fig. 4. Only Ag, P, O, Ta and N elements were detected in the XPS survey spectrum (Fig. 4a) and no peaks corresponding to other elements were observed. The binding energies for the Ta 4f5/2, Ta 4f7/2 and N 1s peaks at 27.1, 25.3 and 396.8 eV are typical values for Ta^{5+} and N^{3-} in Ta_3N_5. The binding energy of 403.9 eV assigned to Ta 4p2/3 indicates that some portion of the Ta-N bonds form.[31] The binding energies for the Ag 3d5/2, Ag 3d3/2, P 2p3/2 and P 2p1/2 peaks located at 367.7, 373.7, 132.3 and 133.5 eV are typical values for Ag^+ and PO_4^{3-} in Ag_3PO_4. The O 1s peak centered at 530.4 eV was associated with the O^{2-} in Ag_3PO_4. The other O 1s peak at 532.2 eV was associated with the presence of an -OH group or a water molecule on the surface of the Ag_3PO_4/Ta_3N_5 composite.[30]

Photocatalytic performance and photostability under visible light irradiation

The optical absorption property of Ag_3PO_4/Ta_3N_5 was investigated with the UV-Vis spectra, as shown in Fig. 5. Pure Ag_3PO_4 exhibits strong absorbance in wavelengths shorter than 500 nm, corresponding to its band gap energy of 2.41 eV. For Ta_3N_5, the absorption edge was found to be at approximately 600 nm. Ag_3PO_4/Ta_3N_5 composite exhibits two absorption edges at 500 and 640 nm, implying a combination of the optical absorption characteristics of Ta_3N_5 and Ag_3PO_4. According to the Kubelka-Munk function,[32] the relationship between the absorption coefficient and the bandgap energy of a semiconductor can be described by the following equation: $\alpha h\nu = A(h\nu - E_g)^{n/2}$, where α, h, n, A, and E_g are the absorption coefficient, Planck's constant, light frequency, proportionality constant and band-gap energy, respectively. The plot of $(\alpha h\nu)^2$ as a function of E_g is shown in Fig. S2. The band gaps for Ag_3PO_4 and Ta_3N_5 are estimated to be 2.41 and 2.11 eV, respectively, which are similar to the values reported previously (2.36 eV for Ag_3PO_4 and 2.1 eV for Ta_3N_5).[33,34] The band gap of the Ag_3PO_4/Ta_3N_5 heterostructure photocatalyst was estimated to be 2.08 eV. The relatively narrow bandgap energy observed for Ag_3PO_4/Ta_3N_5 may be due to the strong interaction in the hybrid structure, which results in more efficient use of the solar spectrum.[30]

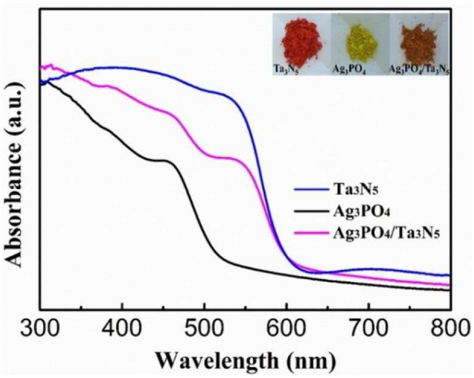

Fig. 5 UV-Vis spectra of the Ag_3PO_4, Ta_3N_5 and Ag_3PO_4/Ta_3N_5 photocatalysts.

The photocatalytic performance of the as-prepared Ag_3PO_4/Ta_3N_5 was evaluated based on the degradation of RhB solution under visible light irradiation without the addition of any sacrificial reagents. For comparison, Ag_3PO_4, and Ta_3N_5 were also studied under the same conditions. Prior to irradiation with light, the suspension solution consisting of RhB and the photocatalyst was magnetically stirred in the dark for 30 min to establish an adsorption-desorption equilibrium (see Fig. S3). Fig. 6a shows the photocatalytic degradation of RhB as a function of irradiation time over different photocatalysts. In the absence of a photocatalyst (blank), direct photolysis of RhB under visible light irradiation could be neglected. The photocatalytic performance of different photocatalysts were in the following order: Ag_3PO_4/Ta_3N_5 > Ag_3PO_4 > Ta_3N_5. For pure Ta_3N_5, the photocatalytic activity is the lowest and the degradation of RhB was only 17% for 10 min. For pure Ag_3PO_4, the degradation of RhB was 96% for 10 min. It is important to note that only 6 min of visible-light irradiation is required for complete degradation of RhB over Ag_3PO_4/Ta_3N_5. The notably enhanced photocatalytic performances of Ag_3PO_4/Ta_3N_5 composite are mainly attributed to more photocatalytic active sites owing to the rough surface and sufficient hetero-interfaces of composite and rapid separation and transfer of charge carriers within the compact hetero-interface between Ag_3PO_4 and Ta_3N_5. The apparent rate constants (k) calculated from the degradation curves of $-\ln(C/C_0)$ as a function of irradiation time are 0.02, 0.26, and 0.63 min^{-1} for Ta_3N_5, Ag_3PO_4 and Ag_3PO_4/Ta_3N_5, respectively (Fig. 6b). The photocatalytic rate of Ag_3PO_4/Ta_3N_5 was approximately 2.5 times that of Ag_3PO_4 and 32 times that of Ta_3N_5. The characteristic absorption band of RhB at approximately 554 nm decreases rapidly under visible light irradiation in the presence of the Ag_3PO_4/Ta_3N_5 photocatalyst and no blue-shift in the absorption band occurred, indicating that the entire conjugated chromophore structure of RhB was easily cleaved. During the photodegradation the absorption band at approximately 200-300 nm also decreases gradually, indicating that the small molecular compounds/intermediates (i.e. benzene ring based species) that were formed during the reaction were also degraded (Fig. S4).[35] Furthermore, the photodegradation curves of Ag_3PO_4/Ta_3N_5 composite photocatalyst with different atom ratio (1:1 and 4:1) are also provided in supporting information (Fig. S5). It is found that 3:1 mole ratio of Ag_3PO_4 to Ta_3N_5 results in the best photodegradation performance among a series of mole ratios of 1:1, 3:1, and 4:1.

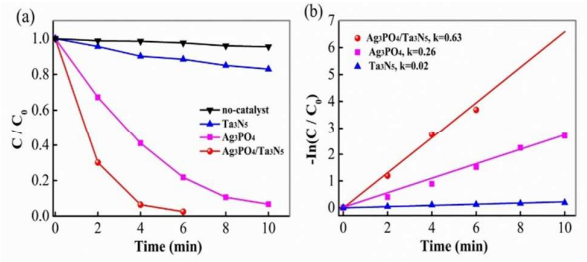

Fig. 6 a) RhB (1×10^{-5}M) photodegradation as a function of illumination time for the Ta_3N_5, Ag_3PO_4, and Ag_3PO_4/Ta_3N_5 photocatalysts and no catalyst. b) Plot of $-\ln(C/C_0)$ as a function of time. (C_0 is the initial concentration of RhB prior to irradiation, and C is the concentration at the specified irradiation time.)

In addition to the photocatalytic activity, the stability of the photocatalysts is another important issue for practical application. To investigate the stability of bare Ag_3PO_4, Ta_3N_5 and Ag_3PO_4/Ta_3N_5, three runs of cycling photodegradation experiments under identical conditions were performed (Fig. 7). The photocatalytic efficiency of pure Ag_3PO_4 decreases as the color changes from an initial yellow color to a dark yellow color after three cycles. This result indicated that bare Ag_3PO_4 photocatalyst was unstable owing to the formation of metallic Ag^0 species resulting from the reduction of Ag^+ from Ag_3PO_4 by photoinduced electrons during the photocatalytic process.[36] This was also evidenced by XRD pattern of the Ag_3PO_4 sample after three cycles, which clearly displayed a weak XRD diffraction peak at around 38 ° indexed to the (111) lattice plane of metallic Ag (see Fig. 8). In contrast, the photocatalytic activity of Ag_3PO_4/Ta_3N_5 maintains a high level of activity during the cycling degradation of RhB. In addition, no metallic Ag was detected after three successive experimental runs in the Ag_3PO_4/Ta_3N_5 system (Fig. 8), which demonstrates the good photostability of the Ag_3PO_4/Ta_3N_5 composite. The above results manifest that the introduction of Ta_3N_5 nanorod aggregates as the support for the Ag_3PO_4 could efficiently prevent the formation of Ag nanoparticles on the surface of Ag_3PO_4 by the construction of compact hetero-interface between Ag_3PO_4 and Ta_3N_5. The detailed reasons for the enhancement of the Ag_3PO_4/Ta_3N_5 photocatalyst associated with activity and stability will be discussed in the following section.

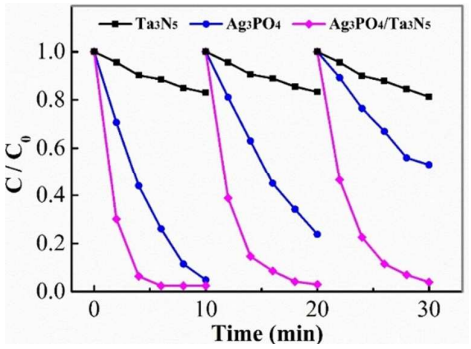

Fig. 7 Recycling tests of the Ta_3N_5, Ag_3PO_4 and Ag_3PO_4/Ta_3N_5 photocatalysts for the degradation of RhB (1×10^{-5}M).

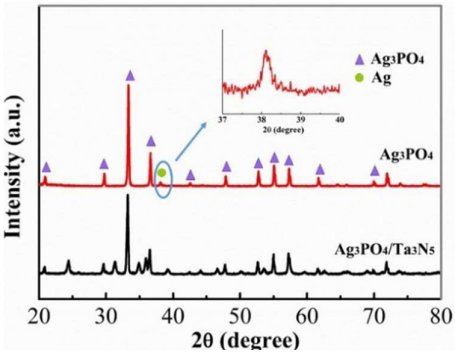

Fig. 8 XRD patterns of Ag_3PO_4 and Ag_3PO_4/Ta_3N_5 photocatalysts after 3 cycles.

Mechanism for the improved photocatalytic activity and stability of Ag_3PO_4/Ta_3N_5

The above experimental results and discussions demonstrate that the photocatalytic activity and stability of Ag_3PO_4 can be improved via coupling Ag_3PO_4 with Ta_3N_5 nanorod aggregates, which is primarily due to the effective charge separation and transfer of photoinduced electrons and holes by the internal build-in field in the p-n junction region. One direct piece of evidence is that the PL intensity of the Ag_3PO_4/Ta_3N_5 photocatalyst is much lower than that of the Ag_3PO_4 sample (see Fig. 9), indicating that the recombination of the photoexcited electron-hole on the Ag_3PO_4 surface is suppressed due to the formation of a heterojunction between Ag_3PO_4 and Ta_3N_5.[18] EIS is a powerful characterization technique for studying the interfacial charge-transfer properties of photocatalyst.[37] In this study, EIS spectra measurements were performed. The semicircle at high frequency is characteristic of the charge transfer process and the diameter of the semicircle represents the charge transfer resistance. In Fig. 10, the arc for Ag_3PO_4/Ta_3N_5 is much smaller than that for Ag_3PO_4 and Ta_3N_5 under illumination, suggesting that Ag_3PO_4/Ta_3N_5 has a smaller electronic transmission resistance, and a higher efficient charge separation/transfer. On one hand, the compact hetero-interface formed with submicron-sized Ag_3PO_4 and Ta_3N_5 nanorod aggregates could serve as a bridge and provide barrier-free access to transport photo-induced carriers (electrons and holes) between Ag_3PO_4 and Ta_3N_5 during the photcatalytic process, hence greatly improving the separation efficiency of the electrons and holes. On the other hand, the internal build-in fields existing in the hetero-interface could also be beneficial to separate and transfer the electrons and holes within the hybrid composite.[27] Therefore, the efficiency of the photocatalytic degradation of RhB dyes over the Ag_3PO_4/Ta_3N_5 sample is much better.

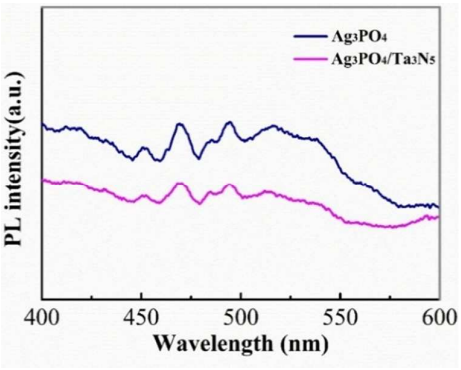

Fig. 9 Photoluminescence spectra of Ag_3PO_4 and Ag_3PO_4/Ta_3N_5.

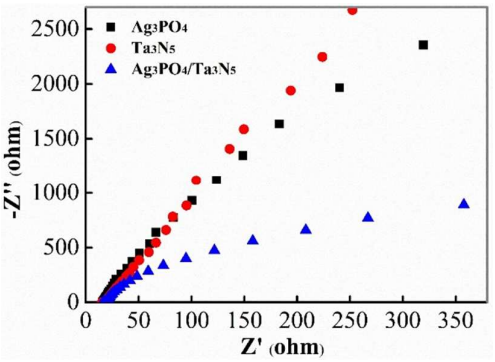

Fig. 10 EIS patterns of the Ag_3PO_4, Ta_3N_5 and Ag_3PO_4/Ta_3N_5 photocatalysts.

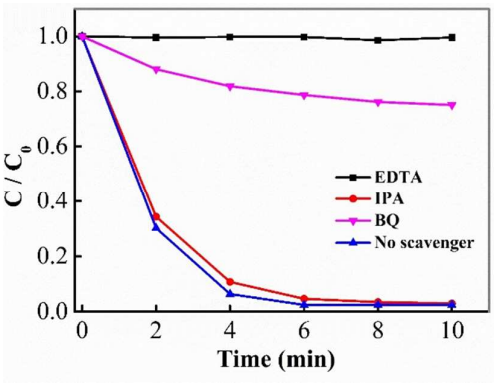

Fig. 11 Photocatalytic activities of the Ag_3PO_4/Ta_3N_5 photocatalyst for the degradation of RhB (1×10^{-5}M) in the presence of different scavengers.

To elucidate the photocatalytic reaction mechanism, we attempted to examine the main reactive species including h^+, $O_2^{-\bullet}$ and •OH that are involved in the photocatalytic process. In the experiments, disodium ethylenediaminetetraacetate (EDTA), benzoquinone (BQ), and isopropanol (IPA) that acted as the scavengers for h^+, $O_2^{-\bullet}$ and •OH were separately introduced into the photocatalytic reaction processes.[33] Fig. 11 shows a comparison of the photocatalytic activity of the Ag_3PO_4/Ta_3N_5 sample for the degradation of RhB in the presence of different scavengers. The addition of EDTA (h^+ scavenger) in the RhB solution results in fast deactivation of Ag_3PO_4/Ta_3N_5 for the degradation of RhB. When BQ ($O_2^{-\bullet}$ scavenger) was added, the efficiency of the photocatalytic degradation decreased substantially. However, the addition of IPA (hydroxyl radical scavenger) has little effect on the photocatalytic activity. These results indicate that in the photocatalytic reaction process of Ag_3PO_4/Ta_3N_5, h^+ and $O_2^{-\bullet}$ are the main reactive oxidizing species, and •OH may only play a less important role. The valence band (VB) edge potential of Ag_3PO_4 (2.81 eV) is close to E^θ (•OH/H_2O) (2.68 eV) and its conduction band (CB) edge potential (0.45 eV) is less negative than E^θ ($O_2/O_2^{-\bullet}$) (0.13 eV).[33] Therefore, for pure Ag_3PO_4, it is difficult for holes to directly oxidize H_2O molecules into •OH radicals, and electrons cannot directly reduce O_2 molecules into $O_2^{-\bullet}$ radicals. However, the CB edge potential (-0.5 eV) of Ta_3N_5 is more negative than E^θ ($O_2/O_2^{-\bullet}$) (0.13 eV), and

the photogenerated electrons from Ta_3N_5 can reduce O_2 to $O_2^{-\bullet}$ through a one-electron reduction reaction. Therefore, for Ag_3PO_4/Ta_3N_5, h^+ and $O_2^{-\bullet}$ are the main reactive oxidizing species in the photocatalytic reaction process.

Based on our experimental results and analysis, a possible pathway for the degradation of dye pollutants by the p-Ag_3PO_4/n-Ta_3N_5 heterojunction photocatalyst is shown in Fig. 12. The Ag_3PO_4 and Ta_3N_5 in the Ag_3PO_4/Ta_3N_5 system act as two photosensitizers responsive to visible light. Under visible irradiation, the absorption of photons by Ag_3PO_4 and Ta_3N_5 leads to excitation of the electrons from their separated VB to CB, leaving holes in the VB. Due to the existence of a built-in electrical potential at the p-n junction, the transfer from the electrons in the CB of Ta_3N_5 to the CB of Ag_3PO_4 is suppressed. However, the electron transfer path from the CB of Ag_3PO_4 to the VB of Ta_3N_5 is feasible. Therefore, the photoinduced electrons and holes are efficiently separated between Ag_3PO_4 and Ta_3N_5. In addition, the photogenerated electrons move easily towards the surface of Ta_3N_5, and react with adsorbed O_2 to form reactive oxygen species such as $O_2^{-\bullet}$. The photoinduced holes may shift to the surface of Ag_3PO_4 to oxidize RhB. Therefore, this fabricated p-n heterojunction Ag_3PO_4/Ta_3N_5 photocatalyst exhibits high photocatalytic activity and stability under visible light radiation.

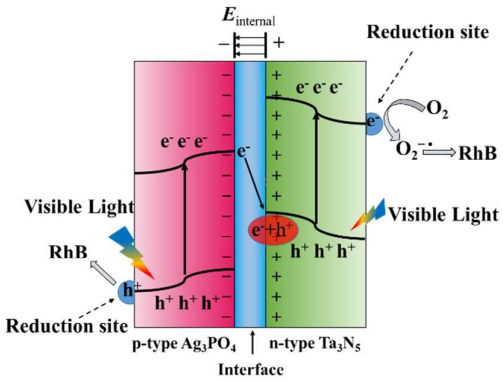

Fig. 12 Schematic illustration of the band alignments and the corresponding proposed charge separation and transfer of p-n heterostructure Ag_3PO_4/Ta_3N_5 composite under visible light irradiation.

Conclusions

In summary, a novel 3D p-n heteroarchitecture Ag_3PO_4/Ta_3N_5 composite has been successfully synthesized by a facile and reproducible in situ temple-free precipitation process. The heteroarchitecture Ag_3PO_4/Ta_3N_5 composite exhibits excellent optical absorption property attributed to double visible-light-response characteristics and matched energy bandgaps of the two components. The unique 3D heteroarchitecture provides sufficient hetero-interfaces to form internal build-in field in the p-n heterojunction region between Ag_3PO_4 and Ta_3N_5, which greatly improve the charge separation efficiency and transfer of photogenerated electrons and holes. Owing to these beneficial features, Ag_3PO_4/Ta_3N_5 composites exhibited excellent photocatalytic activity and stability for the degradation of RhB, superior to those of pure Ta_3N_5 and Ag_3PO_4 under visible light irradiation (≥420 nm). Reactive oxidative species detection studies indicated that the photodegradation of RhB over Ag_3PO_4/Ta_3N_5 under visible light is primarily via holes and $O_2^{-\bullet}$ radicals. Our work provides a highly efficient p-n heterojunction Ag_3PO_4/Ta_3N_5 photocatalyst via a fabrication approach that may be beneficial for the development of other heterostructure photocatalysts.

Experimental Section

Materials

All of the chemicals used in this study were of analytical grade and used without further purification. Ethanol, hydrogen peroxide (H_2O_2) and hydrofluoric (HF) acid were supplied by Sinopharm Chemical Reagent Beijing Co. (Beijing, China). Tantalum powders (99.9%), silver nitrate ($AgNO_3$), and disodium dihydrogen phosphate hydrate ($Na_2HPO_4{\cdot}12H_2O$), were supplied by Aladdin. Ammonia gas was supplied by Haipu Gas (Beijing, China) Co. Ltd. Rhodamine B (RhB) was purchased from Fisher Scientific (Hong Kong) Co., Ltd. Deionized (DI) water was used in all of the experiments.

Preparation of heterostructure Ag_3PO_4/Ta_3N_5 composite

Ta_2O_5 was prepared via a facile hydrothermal process. In a typical procedure, 0.5 g of tantalum powder (99.9%, black-color) was added to 50 mL of a 0.5 mol L^{-1} aqueous hydrofluoric acid solution with 12 mL of a 30 wt% hydrogen peroxide solution under stirring for 10 min. Then, the mixture was loaded into a Teflon-lined autoclave for thermal treatment at 240 °C for 12 h. After cooling, Ta_2O_5 was obtained by filtration followed by rinsing with ethanol and drying at 60 °C for 12 h. Next, Ta_3N_5 was obtained via thermal nitridation of the homemade Ta_2O_5 powder at 850 °C for 6 h under an ammonia gas flow (40 mL min^{-1}). Then, the nitridation reaction was allowed to cool to room temperature in the presence of the ammonia flow.

The Ag_3PO_4/Ta_3N_5 composites were obtained by immersing homemade Ta_3N_5 nanorods into an $AgNO_3$ solution followed by phosphorylation in an aqueous Na_2HPO_4 medium. Typically, an appropriate amount of Ta_3N_5 powder was suspended in an aqueous $AgNO_3$ solution followed by stirring at room temperature for 1 h. In addition, 10 mL of a 0.15 M aqueous Na_2HPO_4 solution was dropped into the previously mentioned suspended solution and stirred for 3 h. The obtained product (i.e., Ag_3PO_4/Ta_3N_5) was collected by washing and drying. For comparison, a pure Ag_3PO_4 sample was also prepared using the same procedure without the addition of Ta_3N_5.

Characterizations

The phase structure of the samples was characterized by X-ray diffraction (XRD) on a Rigaku D/max 2500 VB2+/PC diffractometer using Cu K radiation (λ = 0.15406 nm) at 40 kV and 40 mA. The morphologies of the samples were examined by scanning electron microscopy (SEM) (JEOL JSM-6701F) and transmission electron microscopy (TEM) (JEOL JEM-3010). X-ray photoelectron spectroscopy (XPS) was performed on a Thermo ESCALAB250 X-ray photoelectron spectrometer using Al Ka as an X-ray source. The optical properties of Ag_3PO_4/Ta_3N_5 were studied using the adsorption spectra recorded on a UV-Vis spectrophotometer

(Lambda 950 UV/VIS). The photoluminescence (PL) spectra were obtained on a Hitachi F7000 at an excitation wavelength of 315 nm.

Photocatalytic activity measurement

The photocatalytic activities of the sample photocatalysts were evaluated based on the degradation of RhB under visible light irradiation. In a typical process, 30 mg of the photocatalyst were added to 80 mL of RhB (1×10^{-5}M). Prior to irradiation, the suspension was stirred in the dark for 30 min to establish adsorption-desorption equilibrium. Then, the suspension was exposed to a 300 W Xe lamp with an ultraviolet cutoff filter (providing visible light λ≥420 nm) under magnetic stirring. At 2 min intervals of visible light irradiation, 3 mL of the suspension was collected and then centrifuged to remove the photocatalyst particles. The concentration of RhB was determined by measuring the maximum absorption peak at 554 nm with a UV-Vis spectrophotometer.

Photoelectrochemical characterization of Ag_3PO_4/Ta_3N_5

Electrochemical impedance spectroscopy (EIS) was performed using an electrochemical workstation (CHI660C, ShangHai) operating in a standard three electrode configuration with Ag_3PO_4/Ta_3N_5, saturated calomel electrode (SCE), and Pt wire as the working, reference, and counter electrode, respectively. The supporting electrolyte was a 0.5 M Na_2SO_4 solution. The visible light source was obtained from a 300 W Xe lamp with a 420 nm cut-off filter. The working electrodes were prepared using the dipping method on indium-tin oxide (ITO) conductive glass. Briefly, 0.3 g of the photocatalyst and 10 mL of isopropyl alcohol were mixed for 1 h and dipped on the ITO glass to form a uniform film. Then, the Ag_3PO_4/Ta_3N_5 electrodes were obtained after storing the film in a vacuum at 80 °C for 2 h.

Detection of reactive oxidative species

The reactive oxidative species in the photodegradation were detected using in situ trapping experiments. The detection process is similar to the photodegradation experimental process. Three different scavengers, such as p-benzoquinone (BQ, $O_2^{-\bullet}$ radicals scavenger), disodium ethylenediaminetetraacetate (EDTA, holes scavenger) and isopropanol (IPA, •OH radicals scavenger), were added to the RhB solution prior to illumination in three separated photodegradation systems. The concentration of the scavengers was set at 1.0 mM.

Acknowledgements

The work was supported by the National Natural Science Foundation of China (Nos. 21176019, 21377011, 21476019), specialized research fund for the Doctoral program of higher education of China (20110010110002), and Beijing Higher Education Young Elite Teacher Project (YETP0487).

Notes and references

1 A. Kubacka, M. Fernandez-Garcia, G. Colon, *Chem. Rev.*, 2012, **112**, 1555-1614.
2 H. Tong, S.X. Ouyang, Y.P. Bi, N. Umezawa, M. Oshikiri, J.H. Ye, *Adv. Mater.*, 2012, **24**, 229-251.
3 P. Wang, B.B. Huang, X.Y. Qin, X.Y. Zhang, Y. Dai, J.Y. Wei, M.H. Whangbo, *Angew. Chem. Int. Ed.*, 2008, **47**, 7931-7933.
4 C. Hu, T.W. Peng, X.X. Hu, Y.L. Nie, X.F. Zhou, J.H. Qu, H. He, *J. Am. Chem. Soc.*, 2010, **132**, 857-862.
5 B. Wang, X.Q. Gu, Y.L. Zhao, Y.H. Qiang, *Appl. Surf. Sci.*, 2013, **283**, 396-401.
6 Y.S. Xu, W.D. Zhang, *Dalton Trans.*, 2013, **42**, 1094-1101.
7 G. Fu, G. Xu, S. Chen, L. Li. M. Zhang, *Catal. Commun.*, 2013, **40**, 120-124.
8 Z. Cui, M. Si, Z. Zheng, L. Mi, W. Fa, H. Jia, *Catal. Commun.*, 2013, **42**, 121-124.
9 Z. Wang, B. Huang, Y. Dai, X. Qin, X. Zhang, P. Wang, H. Liu, J. Yu, *J. Phys. Chem. C*, 2009, **113**, 4612-4617.
10 L. Yu, Y. Huang, G. Xiao, D. Li, *J. Mater. Chem. A*, 2013, **1**, 9637-9640.
11 Y. Bi, S. Ouyang, J. Cao, J. Ye, *Phys. Chem. Chem. Phys.*, 2011, **13**, 10071-10075.
12 Y. Liu, L. Fang, H. Lu, L. Liu, H. Wang, C. Hu, *Catal. Commun.*, 2012, **17**, 200-204.
13 Z. Yi, J. Ye, N. Kikugawa, T. Kako, S. Ouyang, H. Stuart-Williams, H. Yang, J. Cao, W. Luo, Z. Li, Y. Liu, R. L. Withers, *Nat. Mater.*, 2010, **9**, 559-564.
14 H. Li, Y. Zhou, W. Tu, J. Ye, Z. Zou, *Adv. Funct. Mater.*, 2015, DOI: 10.1002/adfm.201401636.
15 W. Yao, B. Zhang, C. Huang, C. Ma, X. Song, Q. Xu, *J. Mater. Chem.*, 2012, **22**, 4050-4055.
16 G. Li, L. Mao, *RSC Adv.*, 2012, **2**, 5108-5111.
17 L. Zhang, H. Zhang, H. Huang, Y. Liu, Z. Kang, *New J. Chem.*, 2012, **36**, 1541-1544.
18 Q. Xiang, D. Lang, T. Shen, F. Liu, *Appl. Catalysis B: Environ.*, 2015, **162**, 196-203.
19 R. Asahi, T. Morikawa, T. Ohwaki, K. Aoki, Y. Taga, *Science*, 2001, **293**, 269-271.
20 G. Hitoki, A. Ishikawa, T. Takata, J.N. Kondo, M. Hara, K. Domen, *Chem. Lett.*, 2002, **31**, 736-737.
21 G. Hitoki, T. Takata, J.N. Kondo, M. Hara, H. Kobayashi, K. Domen, *Chem. Commun.*, 2002, **16**, 1698-1699.
22 F. Zhang, A. Yamakata, K. Maeda, Y. Moriya, T. Takata, J. Kubota, K. Teshima, S. Oishi, K. Domen, *J. Am. Chem. Soc.*, 2012, **134**, 8348-8351.
23 K. Maeda, K. Teramura, D. Lu, T. Takata, N. Saito, Y. Inoue, K. Domen, *Nature*, 2006, **440**, 295-295.
24 K. Maeda, K. Domen, J. Phys. Chem. C, 2007, 111, 7851-7861.
25 D. Yokoyama, H. Hashiguchi, K. Maeda, T. Minegishi, T. Takata, R. Abe, J. Kubota, K. Domen, *Thin Solid Films*, 2011, **519**, 2087-2092.
26 M. Higashi, K. Domen, R. Abe, *Energy Environ. Sci.*, 2011, **4**, 4138-4147.
27 P. Ruankham, L. Macaraig, T. Sagawa, H. Nakazumi, S. Yoshikawa, *J. Phys. Chem. C*, 2011, **115**, 23809-23816.
28 M. Liao, J. Feng, W. Luo, Z. Wang, J. Zhang, Z. Li, T. Yu, .Z. Zou, *Adv. Funct. Mater.*, 2012, **22**, 3066-3074.
29 K. Maeda, D. Lu and K. Domen, *Chem.-Eur. J.*, 2013, **19**, 4986-4991.
30 H. Katsumata, T. Sakai, T. Suzuki, S. Kaneco, *Ind. Eng. Chem. Res.*, 2014, **53**, 8018-8025.
31 Y. Chen, S. Liang , L. Wen, W. Wu, R. Yuan, X. Wang, L. Wu, *Phys. Chem. Chem. Phys.*, 2013, **15**, 12742-12747.
32 J. Zeng, H. Wang, Y.C. Zhang, M.K. Zhu, H. Yang, *J. Phys. Chem. C*, 2007, **111**, 11879-11887.
33 C. Cui, Y. Wang, D. Liang, W. Cui, H. Hu, B. Lu, S. Xu, X. Li, C. Wang, Y. Yang, *Appl. Cataly. B: Environ.*, 2014, **158–159**, 150-160.

34 W.J. Chun, A. Ishikawa, H. Fujisawa, T. Takata, J. N. Kondo, M. Hara, M. Kawai, Y. Matsumoto, K. Domen, *J. Phys. Chem. B*, 2003, **107**, 1798-1803.
35 W. Dong, C. Lee, X. Lu, Y. Sun, W. Hua, G. Zhuang, S. Zhang, J. Chen, H. Hou, D. Zhao, *Appl. Cataly. B: Environ.*, 2010, **95**, 197-207.
36 H. Wang, Y. Bai, J. Yang, X. Lang, J. H. Li, L. Guo, *Chem.-Eur. J.*, 2012, **18**, 5524-5529.
37 F. Fabregat-Santiago, G. Garcia-Belmonte, I. Mora-Sero, J. Bisquert, *Phys. Chem. Chem. Phys.*, 2011, **13**, 9083-9118.